





Kinetic modeling of the chemotactic process in run-and-tumble bacteria

Andrea Villa-Torrealba ^{*}, Simón Navia , and Rodrigo Soto [†]
*Departamento de Física, Facultad de Ciencias Físicas y Matemáticas,
 Universidad de Chile, Avenida Blanco Encalada 2008, Santiago, Chile*

 (Received 11 May 2022; revised 26 February 2023; accepted 14 March 2023; published 28 March 2023)

The chemotactic process of run-and-tumble bacteria results from modulating the tumbling rate in response to changes in chemoattractant gradients felt by the bacteria. The response has a characteristic memory time and is subject to important fluctuations. These ingredients are considered in a kinetic description of chemotaxis, allowing the computation of the stationary mobility and the relaxation times needed to reach the steady state. For large memory times, these relaxation times become large, implying that finite-time measurements give rise to nonmonotonic currents as a function of the imposed chemoattractant gradient, contrary to the stationary regime where the response is monotonic. The case of an inhomogeneous signal is analyzed. Contrary to the usual Keller–Segel model, the response is nonlocal, and the bacterial profile is smoothed with a characteristic length that grows with the memory time. Finally, the case of traveling signals is considered, where appreciable differences appear compared to memoryless chemotactic descriptions.

DOI: [10.1103/PhysRevE.107.034605](https://doi.org/10.1103/PhysRevE.107.034605)

I. INTRODUCTION

The ability of motile microorganisms to sense and migrate along the gradient of an external stimulus or field is known as taxis [1]. Chemotaxis is the most remarkable example; in this case, the migration is due to a chemical or ligand gradient [2,3]. Biological [4–7] as well as artificial [8–11] microswimmers are able to perform chemotaxis. For instance, chemotaxis is a key ingredient in the performance of the immune system to seek and annihilate foreign invaders [12], and for bacteria, it helps in finding their ecological niche.

One of the first theoretical models created to study the chemotaxis phenomenon at the macroscopic level was the Keller–Segel model, which couples a diffusion-drift equation for bacterial density with a reaction-diffusion equation for the chemoattractant concentration and was first developed to describe slime mold agglomeration [13]. Over the years, this model was adapted to describe chemotaxis in run-and-tumble (RT) bacteria [14]. Seyrich *et al.* [15], improved this model, including a sensing threshold and the saturation in the chemotactic response, allowing them to reproduce a traveling bacteria pulse. Other studies considered different ways to merge the bacterial dynamics with the chemoattractant concentration. Saragosti *et al.* [16] studied bacterial waves driven by chemotaxis, involving reaction-diffusion equations derived from a kinetic description without memory of the RT dynamic. Their results are in qualitative agreement with experiments. Taktikos *et al.* [17] inspected the diffusive behavior for several swimming strategies: run-and-tumble, run-and-reverse, and run-reverse-and-flick, from a phenomenological point of view. They introduced the chemotactic effect at the

tumble rate by integrating the concentration and the response function, showing that the RT strategy is more efficient than run-reverse and flick.

Chemotaxis in a typical bacterium such as *Escherichia coli* (*E. coli*) is an extensive topic of study since it not only expresses metabolic preferences but also reveals bias in its motility due to the environment [18,19]. Their motion is tied to the rotation of the bacterial flagellum in the RT dynamics. When all the flagella rotate counterclockwise, they form a well-ordered bundle and propel the bacteria forward in “run” mode. If one or more flagella reverse direction, then the bundle is disrupted, and the bacteria reorient. This is known as a “tumble,” with an average tumbling angle of approximately 70° [17,20].

The internal chemotaxis network of *E. coli* senses and compares temporary changes in the concentration of its chemical environment to which it responds by changing its movement [2,21–23]. This network is sensitive to small relative changes in chemical concentrations and is able to sense different chemical traces, allowing it to migrate to any of them [24,25]. If the concentration increases over time (for example, because the bacteria entered a food-rich region), then the bacteria tend to keep moving in a straight line, tumbling less frequently, resulting in a biased random walk. However, if this remains constant, then the bacteria return at the same tumbling rate [26]. Moreover, a decrease in the average tumbling angle was reported when bacteria move along a chemical gradient than against it [4,27].

In this article, we use the tools of kinetic theory to analyze the chemotactic process of bacteria that present the RT dynamics described above. The paper is organized as follows. In Sec. II, we present the mathematical model that describes how bacteria respond to gradients in the ligands and how the tumbling rate is modified accordingly. The model considers the fluctuations of large amplitude and long memory on the

^{*}aavillat@gmail.com

[†]rsoto@dfi.uchile.cl

tumbling rate, which have been recently measured for *E. coli* [44]. In Sec. III, we introduce the kinetic model and describe the relevant observables that quantify the chemotactic response to ligand gradients. Section IV considers the case of a uniform concentration gradient, obtaining the steady bacterial current and the relaxation times in terms of the microscopic model. The results for a chemotactic signal changing in space and time are explored in Sec. V, with special attention to the spatial distribution of bacteria under a chemotactic landscape or for a localized traveling signal. Conclusions and perspectives are finally given in Sec. VI.

II. CHEMOTACTIC SIGNALING

We will describe bacteria moving in three spatial dimensions but also in two-dimensional conditions, which is usually the case when solid surfaces are present [28]. For the motion of bacteria, we will consider the RT model, where each swimmer moves at a constant speed V in the direction indicated by its director $\hat{\mathbf{n}}$ and performs tumbles with a rate ν . At each tumble, the director changes to a new one $\hat{\mathbf{n}}'$, with a probability that depends only on the relative angle between both directors, $w(\hat{\mathbf{n}} \cdot \hat{\mathbf{n}}')$. Recently, we showed that unless w is quite singular, in the sense that it is highly peaked at 1 and -1 , bacteria reach a diffusive motion after a few tumble events [29]. Then, different functional forms of w only change quantitatively the value of the diffusion coefficient, which for all cases scales as $D \sim V^2/\nu$. Hence, for simplicity, we will consider that the tumble is isotropic, meaning that w is constant [$w = 1/(2\pi)$ in two dimensions and $w = 1/(4\pi)$ in three dimensions]. As usual, translational Brownian diffusivity is not included because it is much smaller than the one that results from the RT dynamics [30]. Finally, rotational diffusion is not included either because contrary to the tumble dynamics, it does not respond to the chemotactic signal. Its inclusion would only produce minor changes in the results.

There is a well-studied biochemical pathway for describing the internal chemotaxis network of *E. coli*, which has rationalized into a set of Langevin equations for the kinase activity $a(t)$, the receptor methylation level $m(t)$, and the relative CheY-P concentration phosphorylated protein with respect to its equilibrium value $y(t)$ [31–34],

$$\dot{a} = -\frac{1}{\tau_a}[a - \bar{a}(m, l)] + \zeta_a, \quad (1)$$

$$\dot{m} = -\frac{1}{\tau_m}a + \zeta_m, \quad (2)$$

$$\dot{y} = -\frac{y}{\tau_y} + \gamma a + \zeta_y, \quad (3)$$

where l is the ligand concentration and ζ_a , ζ_m , and ζ_y are white noise terms, with correlations $\langle \zeta_a(t_1)\zeta_a(t_2) \rangle = 2T_a\delta(t_1 - t_2)$, $\langle \zeta_m(t_1)\zeta_m(t_2) \rangle = 2T_m\delta(t_1 - t_2)$, $\langle \zeta_y(t_1)\zeta_y(t_2) \rangle = 2T_y\delta(t_1 - t_2)$, and vanishing cross-correlations $\langle \zeta_a(t_1)\zeta_m(t_2) \rangle = \langle \zeta_a(t_1)\zeta_y(t_2) \rangle = \langle \zeta_m(t_1)\zeta_y(t_2) \rangle = 0$. T_a , T_m and T_y describes the intensity of the environmental noise, which is not necessarily thermal inside cells for the ligand, methylation level, and CheY-P concentration, respectively. For *E. coli*, the equilibrium kinase activity is $\bar{a} \approx \alpha m - \beta l$, α and β are the coupling constant due to the linear approximation around

the steady-state [34]. The timescales for kinase response τ_a , methylation response τ_m and CheY-P concentration τ_y , are well separated: $\tau_a, \tau_y \ll \tau_m$. Finally, γ accounts for the coupling of CheY-P with the kinase activity. With this, the chemotactic response can be schematized as follows. If there is an instantaneous increase in the ligand concentration, then \bar{a} will decrease, inducing first a decrease on a and y and, on a slower scale, a decrease of m . After a transient of the order of τ_m , the system will reach a new steady state with $a = \bar{a} = 0$, $y = 0$, and $m = \beta l/\alpha$, on average. That is, for a transient, y takes values opposite to the change on l . To finish the chemotactic circuit description, we use the model of Tu and Grinstein [35], where they show that tumbling is an activated process in which the free energy barrier to switch the flagella rotary motor direction depends on y . Assuming that the changes in y are small, a Taylor expansion can be made on the free energy barrier, concluding that $\nu = \nu_0 e^{\chi y}$, where $\chi > 0$ measures the sensibility to changes in CheY-P concentration and ν_0 is the tumbling rate of models without stochasticity, that is, where the tumbling rate is constant over time. With this coupling, an instantaneous increase in the ligand reduces y and the tumbling rate, making bacteria swim for a longer time in the direction of food, resulting in a biased random walk.

The experimental works in Refs. [21,31–34,36,37] show that $\tau_a = 0.02$ s and $\tau_y = 0.5$ s are smaller than $\tau_m = 8$ s. If we consider temporal variations of the ligand concentration on the scale of τ_m , then we can adiabatically eliminate the fast degrees of freedom. To do so, we take the limit $\tau_a \rightarrow 0$ in Eq. (1), resulting in $a = \bar{a} = \alpha m - \beta l$ and the limit $\tau_y \rightarrow 0$ in Eq. (3), resulting in $y = \tau_y \gamma a$. Taking the temporal derivative of these expressions and using Eq. (2) to eliminate m , we obtain $\dot{y} = -y/\tau - \beta \gamma \tau_y \dot{l} + \zeta$, where $\tau = \tau_m/\alpha$ is the relaxation time of the effective chemotactic signaling and ζ is a white noise with correlation $\langle \zeta(t_1)\zeta(t_2) \rangle = 2T\delta(t_1 - t_2)$, with $T = (\tau_y \alpha)^2 (\gamma^2 T_m + T_y/\tau_m^2)$. Finally, it is convenient to define $X = y/\sqrt{T\tau}$, which is a dimensionless Gaussian variable of unit variance that satisfies the equation

$$\dot{X} = -\frac{X + bl}{\tau} + \sqrt{\frac{2}{\tau}}\xi, \quad (4)$$

where $b = \beta \gamma \tau_y \sqrt{\tau/T}$ measures the coupling to the ligand and ξ is a white noise of correlation $\langle \xi(t_1)\xi(t_2) \rangle = \delta(t_1 - t_2)$. For the temporal derivative of l in Eq. (4), we use that the ligand has some spatial-temporal distribution $l(\mathbf{r}, t)$ and, using the chain rule, resulting in the Lagrangian derivative

$$\dot{l} = V\hat{\mathbf{n}} \cdot \nabla l + \frac{\partial l}{\partial t}. \quad (5)$$

In term of these variables, the tumbling rate is

$$\nu = \nu_0 e^{\lambda X}, \quad (6)$$

where $\lambda = \sqrt{T\tau}\chi$ measures the sensitivity of the tumbling rate to changes in X . Besides its natural dependence with χ , it also increases with the memory time and the noise amplitude of CheY-P fluctuations. We remark that this is a description with normalized variables of the phenomenon, made to highlight the influence of the relevant scales, the relaxation time

of the chemotactic signal, τ , and the sensitivity of the tumble rate to the changes in X , λ .

Note that if neglect memory and fluctuations, X follows instantaneously the ligand rate of change, $\dot{X} = -b\dot{l}$, resulting in the tumbling rate $\nu = \nu_0 e^{-\lambda b l}$. This expression, or similar ones reflecting that the tumbling rate is a decreasing function of the ligand intake rate, have been previously used in Refs. [38–42]. In addition, in the literature, the tumble response has been approximated in a linearized form [43] and without including temporal variations of the chemoattractant gradient [14]. Here, we go beyond this approximation, considering the effects of fluctuations and memory. To recover the memoryless limit, it sufficient to take $\tau \rightarrow 0$ in the forthcoming expressions. To neglect the effect of fluctuations ($T \rightarrow 0$), the previous changes of variables imply that we have to simultaneously take the limits $b \rightarrow \infty$, $\lambda \rightarrow 0$, while $b\lambda$ remains constant.

In Ref. [44], by tracking several individual *E. coli* (RP437 bacteria in motility buffer supplemented with serine) in 3D, it was possible to fit the relevant parameters to: $V = 27 \mu\text{m/s}$, $\nu_0 = 0.22 \text{ s}^{-1}$, $\tau = 19 \text{ s}$, and $\lambda = 1.62$. However, in Ref. [32] they obtained $\tau = 8 \text{ s}$ from the study of biochemical networks. The bacterial strains and culture media are different, which could be origin of this difference in values. Nevertheless, they are of the same order, validating the use of the approximations above. The fitted value of λ is rather high, meaning that fluctuations are indeed important (as was noticed in the large variability of tumbling rates in experiments [44]). This large value would imply that a simple linear expansion for the free energy barrier is only a first approximation and higher order terms would be necessary for a full quantitative agreement. However, in the absence of additional experiments, for this study we consider only up to this order, where already interesting results are obtained. Even more, to obtain explicit results, in Sec. V we will consider the additional approximation $\nu \approx \nu_0(1 + \lambda X)$. The description of the chemotactic coupling, which is finally expressed in Eq. (4), requires that X does not deviate strongly from its equilibrium value, implying that the ligand gradients should not be too large. Also, for the validity of the adiabatic elimination, the temporal variations of the ligand must take place in scales larger than τ_a and τ_y .

Finally, in what follows, to simplify the resulting expressions, we will fix dimensions such that $V = \nu_0 = b = 1$, also implying that lengths are measured in units of the mean distance traveled by a swimmer between tumbles. In these dimensionless units, the memory time for *E. coli*, according to the experiments in Ref. [44] is $\tau = 4.2$. We recall that this value is specific for *E. coli* with the specified culture conditions. Hence, to maintain the analysis as general as possible, we will present results for small and large values of τ .

III. KINETIC THEORY DESCRIPTION

For simplicity, in what follows, we will present the derivations in three dimensions, but the main results will be given also for two dimensions. Whenever possible, the results will be presented in compact form in terms of the spatial dimensionality $d = 2, 3$. Each bacterium is described by its position $\mathbf{r} = (x, y, z)$, director $\hat{\mathbf{n}} = (\sin \theta \cos \varphi, \sin \theta \sin \varphi, \cos \theta)$, where θ and φ are the standard spherical coordinates, and

the normalized concentration of CheY-P X . Hence, an ensemble of bacteria is described by the distribution function $f(\mathbf{r}, \hat{\mathbf{n}}, X, t)$, normalized such that the integral over \mathbf{r} , $\hat{\mathbf{n}}$, and X gives the total number of bacteria. With these elements, we can write a kinetic equation for the distribution function $f(\mathbf{r}, \hat{\mathbf{n}}, X, t)$

$$\frac{\partial f}{\partial t} + V \hat{\mathbf{n}} \cdot \nabla f = \frac{1}{\tau} \left[\frac{\partial^2 f}{\partial X^2} + \frac{\partial(Xf)}{\partial X} + b l \frac{\partial f}{\partial X} \right] + \nu_0 e^{\lambda X} \left[\frac{1}{4\pi} \int_0^{4\pi} f(\mathbf{r}, \hat{\mathbf{n}}', X, t) d^2 \hat{\mathbf{n}}' - f \right], \quad (7)$$

where $d^2 \hat{\mathbf{n}} = \sin \theta d\theta d\varphi$. The terms on the left-hand side represent the streaming of bacteria moving at velocity $V \hat{\mathbf{n}}$. In the first square bracket on the right-hand side are the Fokker–Planck terms associated to the Langevin Eq. (4). Finally, the last two terms on the right-hand side describe the tumbling as a Lorentz-like equation: a gain term of bacteria swimming at any director $\hat{\mathbf{n}}'$ that perform a tumble and end with $\hat{\mathbf{n}}$, and a loss term [45–47]. Importantly, the tumbling rate is not constant but given by Eq. (6).

The two most relevant observables when there are chemotactic signals are the density profile

$$\rho(\mathbf{r}, t) \equiv \int f(\mathbf{r}, \hat{\mathbf{n}}, X, t) d^2 \hat{\mathbf{n}} dX \quad (8)$$

and the bacterial current

$$\mathbf{J}(\mathbf{r}, t) \equiv \int f(\mathbf{r}, \hat{\mathbf{n}}, X, t) V \hat{\mathbf{n}} d^2 \hat{\mathbf{n}} dX. \quad (9)$$

In the absence of any chemotactic signal ($\dot{l} = 0$), the X variable evolves independently of the position and orientation, allowing us to find the solution of the Fokker–Planck sector in the kinetic equation in terms of Hermite polynomials. The steady solution for X , for vanishing concentration gradient, is a simple Gaussian distribution of zero mean and unit variance. Based on this, when the chemotactic signal is present, we propose solutions as the series

$$f(\mathbf{r}, \hat{\mathbf{n}}, X, t) = \frac{e^{-X^2/2}}{\sqrt{2\pi}} \sum_{n=0}^{\infty} H_n(X/\sqrt{2}) f_n(\mathbf{r}, \hat{\mathbf{n}}, t), \quad (10)$$

where H_n is the Hermite polynomial of order n [such that $H_0(x) = 1$, $H_1(x) = 2x$, ...] [48]. With this expansion, owing to the orthogonality condition of the Hermite polynomials, the density and bacterial current are simply given by the first term in the series

$$\rho(\mathbf{r}, t) = \int f_0(\mathbf{r}, \hat{\mathbf{n}}, t) d^2 \hat{\mathbf{n}}, \quad \mathbf{J}(\mathbf{r}, t) = \int f_0(\mathbf{r}, \hat{\mathbf{n}}, t) V \hat{\mathbf{n}} d^2 \hat{\mathbf{n}}. \quad (11)$$

IV. RESPONSE TO A UNIFORM CONCENTRATION GRADIENT

We first consider the simple case of a uniform concentration gradient, where we can show in detail the analytical methods that will be used. The classical chemotactic response, in which a steady current is established, corresponds to finding a stationary and homogeneous solution,

for which $f_n(\mathbf{r}, \hat{\mathbf{n}}, t) = f_n(\hat{\mathbf{n}})$. Fixing the gradient along the z axis, $\nabla l = l' \hat{\mathbf{z}}$, implying that $\hat{l} = l' \cos \theta$, gives after substituting the expansion (10) into Eq. (7),

$$\frac{2^n n!}{\tau} \left[\frac{bl'}{\sqrt{2}} \cos \theta f_{n-1}(\hat{\mathbf{n}}) + n f_n(\hat{\mathbf{n}}) \right] = \sum_{p=0}^{\infty} I_{pn}(\lambda) [g_p - f_p(\hat{\mathbf{n}})], \quad (12)$$

for $n = 0, 1, 2, \dots$, where we used the orthogonality relation of the Hermite polynomials and we defined $f_{-1} = 0$. For the recurrence equation, we defined

$$g_p = \frac{1}{4\pi} \int f_p(\hat{\mathbf{n}}) d^2 \hat{\mathbf{n}} \quad (13)$$

and the matrix

$$\begin{aligned} I_{pn}(\lambda) &= \frac{1}{\sqrt{2\pi}} \int_{-\infty}^{\infty} e^{\lambda X - X^2/2} H_p(X/\sqrt{2}) H_n(X/\sqrt{2}) dX \\ &= e^{\lambda^2/2} \begin{bmatrix} 1 & \sqrt{2}\lambda & \dots \\ \sqrt{2}\lambda & 2(1 + \lambda^2) & \dots \\ \vdots & \vdots & \ddots \end{bmatrix}. \end{aligned} \quad (14)$$

The relations (12) must be understood as equations for the partial distribution functions $f_n(\hat{\mathbf{n}})$, for $n = 0, 1, 2, \dots$, which are obtained in terms of the set of g_n . Imposing the self-consistent relations (13) gives the full solution in terms of $\rho_0 = 4\pi g_0$, the global density of the bacterial suspension. In practice, the series is truncated for a maximum degree n of Hermite polynomials.

Truncating at $n = 0$ gives a vanishing current because this corresponds to maintaining a symmetric Gaussian distribution for X , not responding to the chemotactic signal. For $n \geq 1$ finite currents are obtained. The expressions are involved, particularly for increasing values of n , where more terms are present. However, by the character of the expansion in Hermite polynomials, the series is not convergent for large values of the ligand gradient l' and only the linear response current is adequately obtained (see Fig. 1 for a comparison with numerical simulations). Performing a Taylor series on l' gives $\mathbf{J} = \mu_0 \rho_0 \nabla l$, where the static mobility μ_0 per swimmer can be computed to different numbers of polynomials n :

$$\mu_0 = \frac{1}{d \left(1 + \tau e^{\frac{\lambda^2}{2}} \right)} \hat{\mu}, \quad n = 1, \quad (15)$$

$$\mu_0 = \frac{2 + e^{\frac{\lambda^2}{2}} (1 + \lambda^2) \tau}{d \left[2 + e^{\frac{\lambda^2}{2}} (3 + 2\lambda^2) \tau + e^{\lambda^2} \tau^2 \right]} \hat{\mu}, \quad n = 2. \quad (16)$$

Here $\hat{\mu} = b\lambda$ gives the characteristic value of the mobility. Note that, as expected, if the chemotactic circuit is broken, either because the CheY-P protein does not respond to changes in the ligand ($b = 0$) or because the energy barrier does not change with X ($\lambda = 0$), the current vanishes identically. Importantly, if we consider only the linear dependence on λ [that is, if we approximate $v \approx v_0(1 + \lambda X)$], then it is sufficient to compute up to $n = 1$, and both expressions coincide to $\mu_0 = \hat{\mu}/[d(1 + \tau)]$. Note that this expression corresponds to the limit where fluctuations are neglected. When the memory is neglected, the mobility reduces to $\mu_0 = \hat{\mu}/d$ even if fluctuations are taken into account.

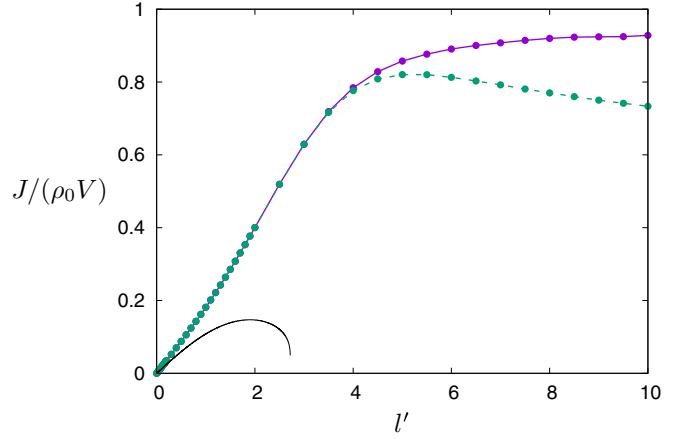


FIG. 1. Normalized stationary current $J/(\rho_0 V)$ for three-dimensional systems with $\tau = 1$ and $\lambda = 1.5$, as a function of the imposed gradient l' . In purple, the stationary current obtained averaging for $T_{\text{avg}} = 2 \times 10^6$ after eliminating the transient, while in green is the averaged response for the shorter time $T_{\text{short}} = 10^2$, starting from an isotropic initial condition. The symbols are the results of the simulations and the colored lines are guides to the eyes. In black, the full nonlinear current keeping terms up to $n = 1$, $J = 2\rho_0 [\arctan \gamma/\gamma - 1]/\log[1 - 2\gamma/(1 + \gamma)]$, where $\gamma = bl\lambda/[1 + \tau e^{\frac{\lambda^2}{2}}]$.

To compare with the analytical predictions, agent-based simulations are performed, solving numerically the differential equations for X and the position vector \mathbf{r} using the Euler–Heun scheme. The tumbles are performed by simulating the Poisson process in discrete time, that is, at each time step Δt , with a probability $\Delta t e^{\lambda X}$, a tumble is performed, and the new direction is chosen at random. For the steady state, after discarding a transient ($T_{\text{transient}} = 10^3$), averages are taken for large times ($T_{\text{avg}} = 2 \times 10^6$). Figure 1 presents some examples of the stationary current as a function of the imposed gradient l' . A first linear response regime is obtained, while for large gradients, the current saturates to the maximum possible value $J_{\text{max}} = \rho_0 V$. From the linear regime, the static motility μ_0 is obtained, which is plotted in Fig. 2 against the theoretical prediction [Eqs. (15) and (16)]. The prediction to order $n = 1$ is accurate for small values of λ and τ , while the following order has an excellent agreement with the simulations up to high values of the parameters, except for small memory, where there is a systematic deviation. Neglecting fluctuations gives a poor result except if τ or λ are small.

With the help of the kinetic equation, it is possible to determine also how long it takes for the system to reach the steady state when, suddenly, a chemotactic signal is established (or when bacteria reach a region with a fixed gradient). For that, we consider that the system starts in equilibrium, that is, homogeneous, isotropic, and with the equilibrium Gaussian distribution for X ,

$$f(\mathbf{r}, \hat{\mathbf{n}}, X, t = 0) = \rho_0 \frac{e^{-X^2/2}}{2(2\pi)^{3/2}}. \quad (17)$$

Using the Laplace transform, $\tilde{A}(s) = \int_0^{\infty} e^{-st} A(t) dt$, the chemotactic mobility when the series is truncated up to $n = 1$,

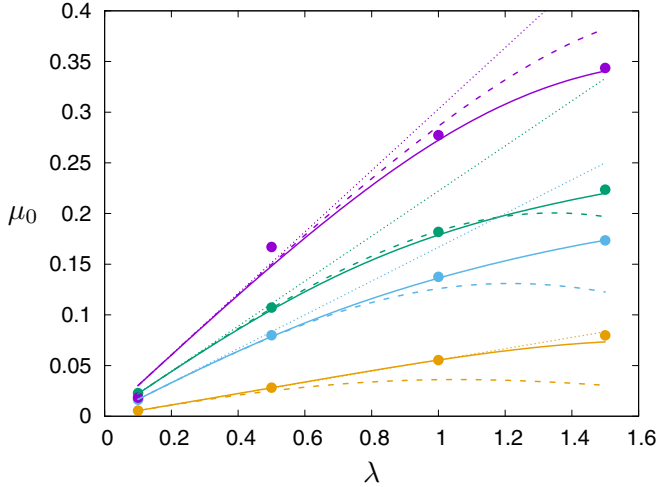


FIG. 2. Static mobility μ_0 that characterizes the linear response as a function of λ , for different values of the memory time τ for three dimensional systems. From top to bottom, $\tau = 0.1$ (purple), 0.5 (green), 1.0 (light blue), and 5.0 (orange). The symbols are the results of the simulation, the dashed lines the theoretical prediction to order $n = 1$ [Eq. (15)], the solid lines the prediction to order $n = 2$ [Eq. (16)], and the dotted lines are the prediction neglecting fluctuations, $\mu_0 = \hat{\mu}/[d(1 + \tau)]$.

is

$$\tilde{\mu}(s) = \frac{\hat{\mu}}{ds[1 + \tau e^{\frac{\lambda^2}{2}} + s\tau(2 + \lambda^2) + e^{-\frac{\lambda^2}{2}}s(1 + s\tau)]}. \quad (18)$$

The poles of $\tilde{\mu}$, which are independent on the spatial dimensionality, give the following relaxation rates to the stationary mobility μ_0 ,

$$v_{1/2} = \frac{2\tau + z \mp \sqrt{z^2 + 4\tau z - 4w}}{2w}, \quad (19)$$

where $w = \tau e^{-\lambda^2/2}$ and $z = \tau\lambda^2 + e^{-\lambda^2/2}$, and the minus (plus) sign should be used for v_1 (v_2). For small λ , $v_1 \propto v_0$ in dimensional units is associated to the relaxation process due to tumbling only, while $v_2 \propto v_0 + 1/\tau$ in dimensional units provides the relaxation to the steady current by the chemotactic circuit besides tumbling.

When more Hermite polynomials are included, new relaxation rates appear. Figure 3 presents the relaxation times $T_i^{\text{relax}} = 1/v_i$ for different memory times τ . For small memory times, the successive relaxation times decrease, with a clear hierarchical structure. This justifies truncating the Hermite series to a few terms, resulting in an adequate description for the slow dynamics; only for a description of the fast relaxations more Hermite terms would be needed. Also, in the small memory regime, the convergence on the values for the relaxation times is fast, and the values are accurately predicted with few terms. When the memory time τ increases, the scale separation of relaxation times and the rapid convergence of the values is lost and more terms are needed to obtain accurate values for the dynamics. Although the description with few terms might be inaccurate for large τ , it still gives new phenomena that result from the finite memory (see Sec. V). Also, we remark that the stationary mobility (Fig. 2) is

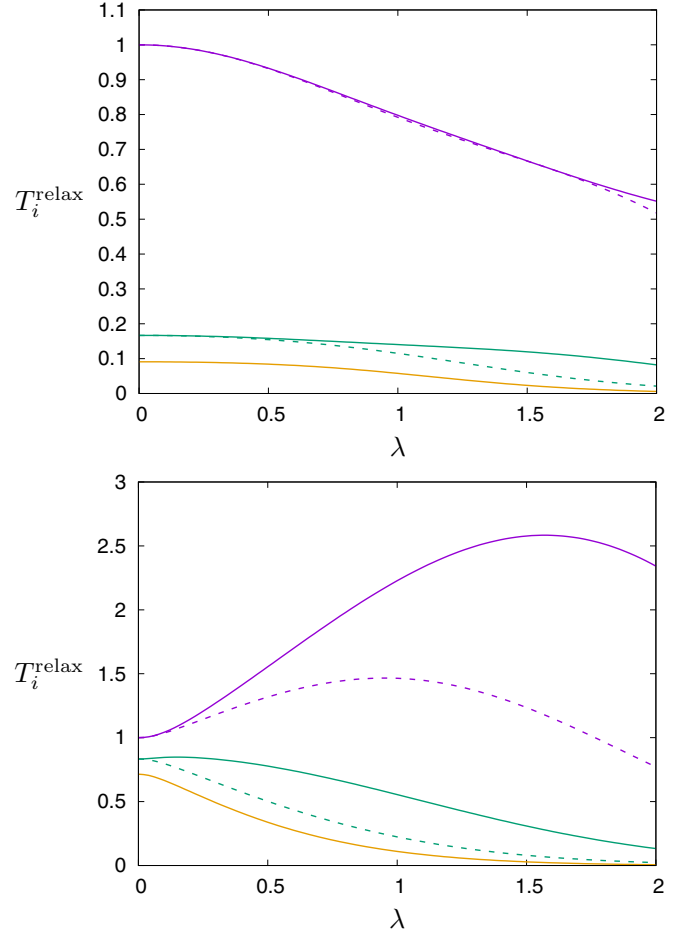


FIG. 3. Largest three relaxation times as a function of λ : T_1^{relax} (purple), T_2^{relax} (green), and T_3^{relax} (orange). The dashed line results using 2 and solid lines using 3 Hermite polynomials. Different memory times are presented: $\tau = 0.2$ (top) and $\tau = 5.0$ (bottom).

accurately described with only two terms even for large values of τ and λ .

The presence of several relaxation times with comparable values for large τ and λ , generates a striking phenomenon. When the system is initiated with an isotropic distribution (equivalently to placing initially the system in a region without chemoattractants), the response, averaged for a short time, can be nonmonotonic with the imposed gradient. Indeed, as shown in Fig. 1, the short-time response presents a maximum as compared to the stationary response, which is strictly monotonic. This nonmonotonicity is due to swimmers that are stuck in suboptimal directions that nevertheless move partially along the gradient ($\cos\theta > 0$), for which the tumbling rate has become very small. Only for much longer times, the swimmers will make tumbles to more optimal directions ($\cos\theta \approx 1$). As a result, the short-time response is also appreciably smaller than the stationary one.

V. SPATIOTEMPORAL RESPONSE

For chemical signals, with spatiotemporal variation, it is relevant to study how the population responds by analyzing the patterns that appear in the bacterial density. Here, we

will consider the linear response of the system, for which we consider that the concentration field of the chemoattractant is given by a reference value plus a small Fourier mode in space and time $l(\mathbf{r}, t) = l_0 + \epsilon l_1 e^{i(\mathbf{k}\cdot\mathbf{r} - \omega t)}$, where $\epsilon \ll 1$. Choosing the z axis along \mathbf{k} gives $\dot{l} = i\epsilon(k \cos \theta - \omega)l_1 e^{i(\mathbf{k}\cdot\mathbf{r} - \omega t)}$. Hence, to solve the kinetic equation we propose a solution

$$f(\mathbf{r}, \hat{\mathbf{n}}, X, t) = f_0(X) + \epsilon f_1(\theta, X) e^{i(\mathbf{k}\cdot\mathbf{r} - \omega t)}, \quad (20)$$

where $f_0(X) = \rho_0 e^{-X^2/2} / [2(2\pi)^{3/2}]$ is the homogeneous and isotropic equilibrium solution, with density ρ_0 , and the perturbation f_1 is expanded as

$$f_1(\theta, X) = \frac{e^{-X^2/2}}{\sqrt{2\pi}} \sum_{n=0}^{\infty} H_n(X/\sqrt{2}) f_n(\theta). \quad (21)$$

Simplifying Eq. (6) to $v = v_0(1 + \lambda X)$, which is valid in the limit of small fluctuations, the kinetic equation to order $\mathcal{O}(\epsilon^1)$

reads

$$i(k \cos \theta - \omega) \left[\frac{\rho_0 b l_1}{2^{3/2} \pi} \delta_{n1} + f_n(\theta) \right] + \frac{n}{\tau} f_n(\theta) - \frac{\lambda}{\sqrt{2}} [g_{n-1} - f_{n-1}(\theta)] - [g_n - f_n(\theta)] - \sqrt{2}(n+1)\lambda [g_{n+1} - f_{n+1}(\theta)] = 0, \quad n = 0, 1, 2, \dots, \quad (22)$$

where g_n are defined in Eq. (13). For the purpose of the linear response, when considering the linear contribution in λ , as in the static regime it is sufficient to truncate the equations to $n = 1$. With this, the bacterial density and current are

$$\rho(\mathbf{r}, t) = \rho_0 + \epsilon \rho_0 \psi(k, \omega) l_1 e^{i(\mathbf{k}\cdot\mathbf{r} - \omega t)}, \quad (23)$$

$$\mathbf{J}(\mathbf{r}, t) = \epsilon \rho_0 \mu(k, \omega) \mathbf{k} l_1 e^{i(\mathbf{k}\cdot\mathbf{r} - \omega t)}, \quad (24)$$

where

$$\psi_{2D}(k, \omega) = \frac{\hat{\mu} [\sqrt{1 + 2\tau\sigma + \tau^2(k^2 + \sigma^2)} - \tau\sqrt{k^2 + \sigma^2} - 1]}{(1 - \sqrt{k^2 + \sigma^2})\sqrt{1 + 2\tau[\sigma - \sqrt{1 + 2\tau\sigma + \tau^2(k^2 + \sigma^2)}] + \tau^2(1 + k^2 + \sigma^2)}} \quad (25)$$

and

$$\psi_{3D}(k, \omega) = \frac{2\hat{\mu} [k\tau + \arctan(k/\sigma)] \arctan[k\tau/(1 + \sigma\tau)] - k\tau \arctan(k/\sigma)}{\tau [k - \arctan(k/\sigma)] [k - \arctan[k\tau/(1 + \sigma\tau)]]} \quad (26)$$

are the density response functions in two and three dimensions, respectively, and to simplify notation we defined $\sigma = 1 - i\omega$. Truncating Eqs. (22) with more terms change the angular distribution, but do not alter the response functions. Using the mass conservation equation $\frac{\partial \rho}{\partial t} = -\nabla \cdot \mathbf{J}$, the current response functions are given by $\mu(k, \omega) = (\omega/k^2)\psi(k, \omega)$. Although formally the linear response functions are valid for all wave vectors and frequencies, in practice, for a given value of l_1 , \dot{l} increases with k and ω . This limits the applicability of the previous expressions up to maximum values of k and ω .

To gain insight, three important cases are considered: the static response, the response to a traveling harmonic wave, and the wake generated by a concentrated traveling chemotactic signal.

A. Static response

For a static chemotactic signal ($\omega = 0$), the response associated to the current, $\mu(k, 0)$, vanishes identically as no stationary current can be produced by a sinusoidal signal in space. The static response function for the density $\psi(k, 0)$ has a bell shape that can be well approximated to a Lorentzian form

$$\psi(k, 0) \approx \frac{\psi_0}{1 + k^2/k_0^2}, \quad (27)$$

with constants that are obtained imposing that the asymptotic limits for $k \ll 1$ and $k \gg 1$ are correctly reproduced. The

results are

$$\psi_{02D} = \frac{\hat{\mu}\tau}{1 + \tau}, \quad k_{02D} = \frac{\sqrt{1 + \tau}}{\tau}, \quad (28)$$

$$\psi_{03D} = \frac{2\hat{\mu}\tau}{1 + \tau}, \quad k_{03D} = \frac{\sqrt{(1 + \tau)(\pi^2 - 4)}}{2\tau}, \quad (29)$$

in two and three dimensions, respectively (see Fig. 4 for a comparison with the full expression). Going back to real

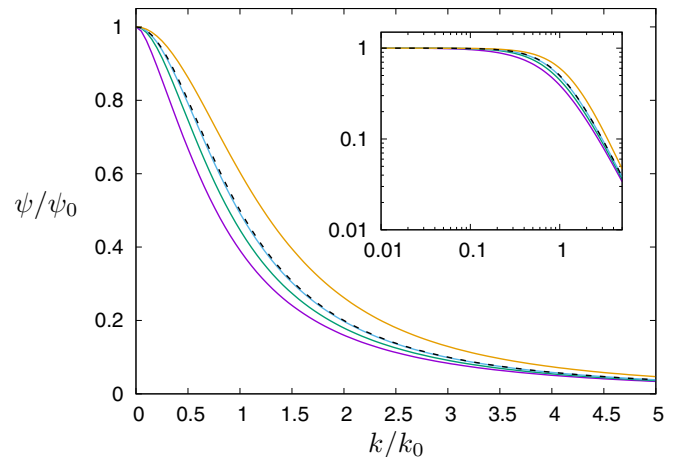


FIG. 4. Comparison of the full expression for the static response function $\psi(k, 0)$ in three dimensions for $\tau = 0.1$ (purple), 0.5 (green), 1.0 (light blue), and 5.0 (orange), with the Lorentzian approximation (black dashed line). In two dimensions the comparison is similar. Inset: the same in log-log scale.

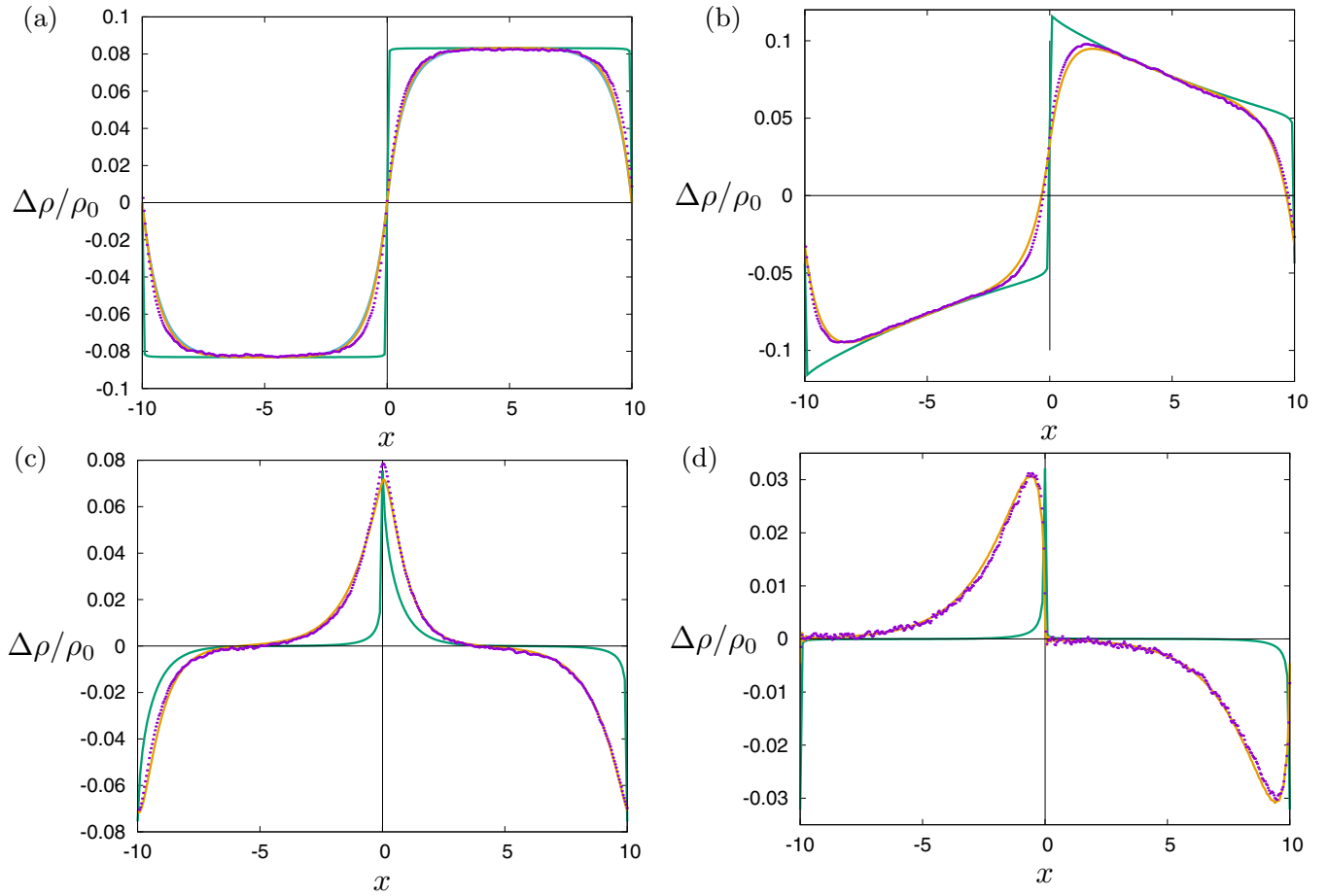


FIG. 5. Stationary normalized density profile in the comoving frame, generated for a propagating square pulse moving at different speeds: (a) $U = 0$, (b) $U = 0.04$, (c) $U = 0.5$, and (d) $U = 1.0$. In purple the results of the simulations of particles with $\tau = 1$ and $\lambda = 1$, moving in two dimensions in a square box of size $L = 20$ with periodic boundary conditions, and with a chemotactic pulse of amplitude $l_1 = 0.4$. In orange the analytical prediction using Eq. (25). For the nonpropagating pulse (a), the prediction using the Lorentzian approximation (27) is shown in light blue. The green curves correspond to the memoryless approximation ($\tau \rightarrow 0$), where the response has been rescaled to put the figures in scale.

space, a concentrated chemotactic signal (a Dirac δ) generates a bacterial cloud with a size k_0^{-1} and total number of swimmers $N_{\text{cloud}} = \rho_0 \psi(0, 0)$, which in 3D equals $2\rho_0 \hat{\mu} \tau / (1 + \tau)$. The characteristic length grows with τ (linear for small values of τ and as the square root for large values), reflecting that bacteria *miss* the chemotactic target because their reaction time depends on the memory time τ . The intensity of the accumulation, ψ_0 , also grows with the memory time, to later saturate.

The nonlocal response given by the density response function $\psi(k, 0)$ should be compared with the usual Keller–Segel model [13]. There, the total current, diffusive plus chemotactic, is $\mathbf{J} = -D\nabla\rho + \rho\mu\nabla l$, and gives for the static regime $\rho = \rho_0 e^{\mu l/D}$, that is, a completely local response.

For a stationary signal with a step profile in one direction, $l(\mathbf{r}, t) = l_0 + l_1 \text{sgn}(x)$, with $\text{sgn}(x) \equiv x/|x|$ the sign function, the stationary bacterial concentration can be explicitly obtained using the Lorentzian approximation

$$\rho(\mathbf{r}) = \rho_0 + l_1 \psi_0 \text{sgn}(x) (1 - e^{-k_0|x|}), \quad (30)$$

resulting in a rounded profile, with the same smoothing length k_0^{-1} .

To test these predictions, we compare with simulations performed with the method described in Sec. IV. In this case, we consider a two-dimensional system, where the particles move in a square box of size $L = 20$, with periodic boundary conditions. To generate an inhomogeneous state, we impose a square ligand profile in the x direction,

$$l_{\text{square}}(x) = \begin{cases} -l_1, & -L/2 \leq x < 0 \\ l_1, & 0 \leq x < L/2 \end{cases}. \quad (31)$$

The system is initialized homogeneously and, after a transient, the particle density $\rho(x)$ is measured. Figure 5(a) shows the normalized density profile $\Delta\rho(x)/\rho = [\rho(x) - \rho_0]/\rho_0$. As the particles are noninteracting, the reference density is immaterial, and smooth profiles are obtained averaging over long times. The theoretical prediction is obtained by numerically evaluating the Fourier series obtained by the multiplication of static response function $\psi(k, 0)$ with the Fourier coefficients of the ligand profile. Both the full expression (25) or the Lorentzian approximation (27) show an excellent agreement with the simulations [Fig. 5(a)]. Note that the rounding off

of the profile, not predicted by the Keller–Segel model, is accurately described by our model.

B. Response to traveling waves

As a second case of interest, we consider ligand waves, traveling with velocity \mathbf{U} . Going to Fourier space, the response is obtained substituting $\omega = \mathbf{k} \cdot \mathbf{U}$ (i.e. $\sigma = 1 - i\mathbf{k} \cdot \mathbf{U}$) in Eqs. (25) and (26). The resulting expressions for ψ and μ , which are no longer isotropic, are complex to work with analytically, but they can be used to compute numerically their inverse Fourier transform and hence the resulting density and current waves.

As a simple condition, we first take the square pulse Eq. (31), moving at constant speed along the x direction: $l_{\text{mov.sq.}}(x, t) = l_{\text{square}}(x - Ut)$. Simulations are performed in two dimensions as in Sec. V A. Here, the particle density $\rho(x)$ is measured in the comoving frame of the wave. Figures 5(b)–5(d) show the normalized density profiles $\Delta\rho(x)/\rho = [\rho(x) - \rho_0]/\rho_0$, which are compared with the theoretical prediction. The agreement is excellent for all the velocities under consideration. For comparison, we present the approximation without memory ($\tau \rightarrow 0$), where we artificially rescaled the response to put the figures in scale. It is seen that, as the Keller–Segel model, this approximation misses the smoothing and rounding off of the profiles observed in the simulations.

As a final case of interest, we consider a localized chemotactic signal that travels through the system with a constant velocity \mathbf{U} , i.e., $l(\mathbf{r}, t) = l_0 + L\delta(\mathbf{r} - \mathbf{U}t)$, where L is the intensity of the signal and δ is the Dirac delta function. The purpose is to analyze the bacterial wake that is generated, which in this case is not homogeneous in y . Figure 6 (top) presents the normalized density $\Delta\rho(\mathbf{r})/(\rho_0\hat{\mu}L)$, obtained by numerically computing the inverse Fourier transform. In simulations, it is not possible to put a Dirac delta signal, and we used instead a Gaussian signal $l(\mathbf{r}) = \frac{L}{2\pi R^2} e^{-r^2/2R^2}$, of width $R = 7$ and intensity $L = 150$, moving in a two dimensional box of size 60×60 . Figure 6 (bottom) shows the generated density wake in the comoving frame, obtained in the simulation. Note that due to the periodicity of the box, the wake appears also in the front. For a moving signal, the total number of particles in the wake vanishes exactly, with an excess of particles near the signal and a deficit at large distances. The limit to vanishing signal velocity is subtle as the crossover distance between these two behaviors diverge when the velocity vanishes.

VI. CONCLUSIONS

We have analyzed the chemotactic process on run-and-tumble bacteria, like *E. coli*. Considering that in the chemotactic signaling pathway there is a dominant timescale, we simplified the mathematical model to a single protein concentration X that controls the tumbling rate as $\nu = \nu_0 e^{\lambda X}$. This protein concentration evolves according to changes of the chemoattractant signal feel by the bacteria while displacing, with a characteristic memory time. With these elements, we have built a kinetic description of a bacterial suspension subject to chemoattractant signals that are either static or have spatiotemporal dependencies. The resulting kinetic equation,

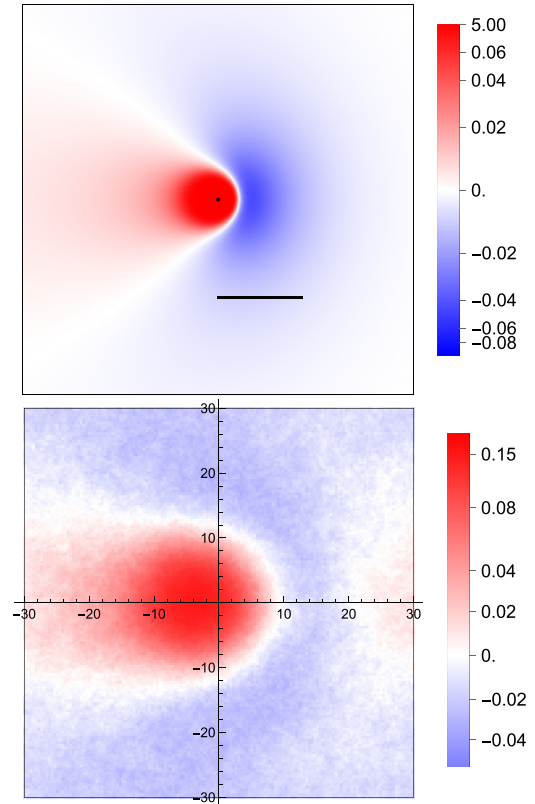


FIG. 6. Top: Prediction for the density wake in two dimensions, generated by a localized chemotactic signal $l(\mathbf{r}, t) = l_0 + L\delta(\mathbf{r} - \mathbf{U}t)$ (black dot), traveling to the right at speed $U = 0.1$ in an unconfined volume. The memory time is $\tau = 1.0$ and the scale bar has length V/v_0 . Bottom: Density wake in two dimensions, obtained in simulations for a Gaussian chemotactic signal $l(\mathbf{r}) = \frac{L}{2\pi R^2} e^{-r^2/2R^2}$, of width $R = 7$ and intensity $L = 150$, traveling to the right at speed $U = 0.1$ in a two dimensional box of size 60×60 . The memory time is $\tau = 1.0$. In both cases, the colorbar, which has a nonlinear scale to facilitate the visualization, presents the normalized density $\Delta\rho(\mathbf{r})/(\rho_0\hat{\mu}L)$.

for the number of bacteria in a given position and orientation and with a specified value of the protein concentration can be solved in Laplace space for the temporal dependence, Fourier spaces for the spatial, and in Hermite polynomials for the protein concentration. In practice, to present the results, the Hermite series are truncated to a few polynomials.

The detailed description of the model allowed us to determine the macroscopic transport coefficients, namely the chemotactic mobility and the density response in terms of the microscopic model. For simplicity and for illustration purposes, we concentrated in the case where the tumbling angle is isotropic. The extension to other tumbling angle distributions is direct, as well as going to higher orders in Hermite polynomials if it were necessary.

The kinetic model shows that there is a well-defined timescale hierarchy when the memory time is small, resulting in a rapid convergence with few Hermite polynomials. However, for larger memory times the hierarchy is broken, implying that the short-time response is quite different to the stationary response, with the former being nonmonotonic

with the chemotactic signal. This result should be taken into account when analyzing experimental data, as long transients can appear.

When spatiotemporal signals are considered, it is found that a natural length scale appears Eq. (28), which for *E. coli* takes the value $k_0^{-1} \approx 170 \mu\text{m}$, when the values measured in Ref. [44] are used. For chemoattractant gradients with characteristic lengths similar or smaller than this value, the simple local response $\mathbf{J} = \mu_0 \rho_0 \nabla I$ breaks down, and the nonlocal kernels (25) and (26), or its approximation (27) should be used.

The analytical and numerical calculations show that relevant features appear in the chemotactic response of run-and-tumble bacteria. These predictions can be exploited in

experimental studies with the aim of validating and refining the models for the chemotactic circuit, as well as new experiments where the different parameters could be measured independently. Possible geometries are microfluidic devices with patterned stationary chemotactic signals, where bacteria can be tracked to measure their concentration around the attractants and the distribution of tumbling rates. Also, stationary flows can be imposed to produce bacterial wakes.

ACKNOWLEDGMENTS

This research is supported by Fondecyt Grants No. 1220536 (R.S.) and No. 3210341 (A.V.-T.) and ANID Millennium Science Initiative Program NCN19_170D, Chile.

-
- [1] T. Krell, J. Lacal, F. Muñoz Martínez, J. A. Reyes-Darias, B. H. Cadirci, C. García-Fontana, and J. L. Ramos, Diversity at its best: Bacterial taxis, *Environ. Microbiol.* **13**, 1115 (2011).
 - [2] H. C. Berg and D. A. Brown, Chemotaxis in *Escherichia coli* analysed by three-dimensional tracking, *Nature* **239**, 500 (1972).
 - [3] H. Stark, Artificial chemotaxis of self-phoretic active colloids: Collective behavior, *Acc. Chem. Res.* **51**, 2681 (2018).
 - [4] O. Pohl, M. Hintsche, Z. Alirezaeizanjani, M. Seyrich, C. Beta, and H. Stark, Inferring the chemotactic strategy of *P. putida* and *E. coli* using modified Kramers–Moyal coefficients, *PLoS Comput. Biol.* **13**, e1005329 (2017).
 - [5] Z. Alirezaeizanjani, R. Großmann, V. Pfeifer, M. Hintsche, and C. Beta, Chemotaxis strategies of bacteria with multiple run modes, *Sci. Adv.* **6**, eaaz6153 (2020).
 - [6] A. C. Grimm and C. S. Harwood, Chemotaxis of *Pseudomonas* spp. to the polyaromatic hydrocarbon naphthalene, *Appl. Environ. Microbiol.* **63**, 4111 (1997).
 - [7] G. Amselem, M. Theves, A. Bae, E. Bodenschatz, and C. Beta, A stochastic description of dictyostelium chemotaxis, *PLoS ONE* **7**, e37213 (2012).
 - [8] I. Theurkauff, C. Cottin-Bizonne, J. Palacci, C. Ybert, and L. Bocquet, Dynamic Clustering in Active Colloidal Suspensions with Chemical Signaling, *Phys. Rev. Lett.* **108**, 268303 (2012).
 - [9] P. M. Vinze, A. Choudhary, and S. Pushpavanam, Motion of an active particle in a linear concentration gradient, *Phys. Fluids* **33**, 032011 (2021).
 - [10] M. N. Popescu, W. E. Uspal, C. Bechinger, and P. Fischer, Chemotaxis of active Janus nanoparticles, *Nano Lett.* **18**, 5345 (2018).
 - [11] O. Pohl and H. Stark, Dynamic Clustering and Chemotactic Collapse of Self-Phoretic Active Particles, *Phys. Rev. Lett.* **112**, 238303 (2014).
 - [12] M. L. Bruce and T. J. Brown, A review of immune system components, cytokines, and immunostimulants in cultured finfish species, *Open J. Anim. Sci.* **07**, 267 (2017).
 - [13] E. F. Keller and L. A. Segel, Initiation of slime mold aggregation viewed as an instability, *J. Theor. Biol.* **26**, 399 (1970).
 - [14] M. J. Tindall, P. K. Maini, S. L. Porter, and J. P. Armitage, Overview of mathematical approaches used to model bacterial chemotaxis II: Bacterial populations, *Bull. Math. Biol.* **70**, 1570 (2008).
 - [15] M. Seyrich, A. Palugniok, and H. Stark, Traveling concentration pulses of bacteria in a generalized Keller–Segel model, *New J. Phys.* **21**, 103001 (2019).
 - [16] J. Saragosti, V. Calvez, N. Bournaveas, A. Buguin, P. Silberzan, and B. Perthame, Mathematical description of bacterial traveling pulses, *PLoS Comput. Biol.* **6**, e1000890 (2010).
 - [17] J. Taktikos, H. Stark, and V. Zaburdaev, How the motility pattern of bacteria affects their dispersal and chemotaxis, *PLoS ONE* **8**, e81936 (2013).
 - [18] G. Rosen, Fundamental theoretical aspects of bacterial chemotaxis, *J. Theor. Biol.* **41**, 201 (1973).
 - [19] J. Adler, Chemotaxis in bacteria, *Science* **153**, 708 (1966).
 - [20] H. C. Berg, *Random Walks in Biology* (Princeton University Press, Princeton, NJ, 1993).
 - [21] S. M. Block, J. E. Segall, and H. C. Berg, Impulse responses in bacterial chemotaxis, *Cell* **31**, 215 (1982).
 - [22] P.-G. de Gennes, Chemotaxis: The role of internal delays, *Eur. Biophys. J.* **33**, 691 (2004).
 - [23] J.-B. Masson, G. Voisinne, J. Wong-Ng, A. Celani, and M. Vergassola, Noninvasive inference of the molecular chemotactic response using bacterial trajectories, *Proc. Natl. Acad. Sci. USA* **109**, 1802 (2012).
 - [24] J. E. Keymer, R. G. Endres, M. Skoge, Y. Meir, and N. S. Wingreen, Chemosensing in *Escherichia coli*: Two regimes of two-state receptors, *Proc. Natl. Acad. Sci. USA* **103**, 1786 (2006).
 - [25] R. Phillips, J. Kondev, J. Theriot, and H. G. Garcia, *Physical Biology of the Cell* (Garland Science, New York, NY, 2013).
 - [26] J. Saragosti, P. Silberzan, and A. Buguin, Modeling *E. coli* tumbles by rotational diffusion. Implications for chemotaxis, *PLoS ONE* **7**, e35412 (2012).
 - [27] J. Saragosti, V. Calvez, N. Bournaveas, B. Perthame, A. Buguin, and P. Silberzan, Directional persistence of chemotactic bacteria in a traveling concentration wave, *Proc. Natl. Acad. Sci. USA* **108**, 16235 (2011).
 - [28] P. D. Frymier, R. M. Ford, H. C. Berg, and P. T. Cummings, Three-dimensional tracking of motile bacteria near a solid planar surface. *Proc. Natl. Acad. Sci. USA* **92**, 6195 (1995).
 - [29] A. Villa-Torrealba, C. Chávez-Raby, P. de Castro, and R. Soto, Run-and-tumble bacteria slowly approaching the diffusive regime, *Phys. Rev. E* **101**, 062607 (2020).
 - [30] H. C. Berg, *E. coli in Motion* (Springer Science & Business Media, Berlin, 2008).

- [31] Y. Tu, T. S. Shimizu, and H. C. Berg, Modeling the chemotactic response of *Escherichia coli* to time-varying stimuli, *Proc. Natl. Acad. Sci. USA* **105**, 14855 (2008).
- [32] F. Tostevin and P. Rein ten Wolde, Mutual Information Between Input and Output Trajectories of Biochemical Networks, *Phys. Rev. Lett.* **102**, 218101 (2009).
- [33] G. Lan, P. Sartori, S. Neumann, V. Sourjik, and Y. Tu, The energy–speed–accuracy trade-off in sensory adaptation, *Nat. Phys.* **8**, 422 (2012).
- [34] S. Ito and T. Sagawa, Maxwell’s demon in biochemical signal transduction with feedback loop, *Nat. Commun.* **6**, 7498 (2015).
- [35] Y. Tu and G. Grinstein, How white Noise Generates Power-Law Switching in Bacterial Flagellar Motors, *Phys. Rev. Lett.* **94**, 208101 (2005).
- [36] V. Sourjik and H. C. Berg, Receptor sensitivity in bacterial chemotaxis, *Proc. Natl. Acad. Sci. USA* **99**, 123 (2002).
- [37] J. E. Segall, S. M. Block, and H. C. Berg, Temporal comparisons in bacterial chemotaxis, *Proc. Natl. Acad. Sci. USA* **83**, 8987 (1986).
- [38] M. J. Schnitzer, Theory of continuum random walks and application to chemotaxis, *Phys. Rev. E* **48**, 2553 (1993).
- [39] K. C. Chen, R. M. Ford, and P. T. Cummings, Cell balance equation for chemotactic bacteria with a biphasic tumbling frequency, *J. Math. Biol.* **47**, 518 (2003).
- [40] E. Lushi, R. E. Goldstein, and M. J. Shelley, Collective chemotactic dynamics in the presence of self-generated fluid flows, *Phys. Rev. E* **86**, 040902(R) (2012).
- [41] T. V. Kasyap and D. L. Koch, Chemotaxis Driven Instability of a Confined Bacterial Suspension, *Phys. Rev. Lett.* **108**, 038101 (2012).
- [42] T. V. Kasyap and D. L. Koch, Instability of an inhomogeneous bacterial suspension subjected to a chemoattractant gradient, *J. Fluid Mech.* **741**, 619 (2014).
- [43] R. N. Bearon and T. J. Pedley, Modeling run-and-tumble chemotaxis in a shear flow, *Bull. Math. Biol.* **62**, 775 (2000).
- [44] N. Figueroa-Morales, R. Soto, G. Junot, T. Darnige, C. Douarce, V. A. Martinez, A. Lindner, and E. Clément, 3D Spatial Exploration by *E. coli* Echoes Motor Temporal Variability, *Phys. Rev. X* **10**, 021004 (2020).
- [45] D. Saintillan, The dilute rheology of swimming suspensions: A simple kinetic model, *Exp. Mech.* **50**, 1275 (2010).
- [46] R. Soto, *Kinetic Theory and Transport Phenomena*, Oxford Master Series in Physics (Oxford University Press, Oxford, UK, 2016).
- [47] D. Saintillan, Rheology of active fluids, *Annu. Rev. Fluid Mech.* **50**, 563 (2018).
- [48] G. B. Arfken and H. J. Weber, *Mathematical Methods for Physicists* (American Association of Physics Teachers, College Park, MD, 1999).